INSTITUTE OF PHYSICS PUBLISHING MEASUREMENT SCIENCE AND TECHNOLOGY

Meas. Sci. Technol. **16** (2005) 2193–2200 doi:10.1088/0957-0233/16/11/009

Electrical conductivity measurement of metal plates using broadband eddy-current and four-point methods

Nicola Bowler and Yongqiang Huang

Center for Nondestructive Evaluation, Iowa State University, Applied Sciences Complex II, Ames, IA 50011, USA

E-mail: nbowler@iastate.edu

Received 1 April 2005, in final form 1 August 2005
Published 28 September 2005
Online at stacks.iop.org/MST/16/2193

Abstract

Electrical conductivity of metal plates is measured by two distinct methods and the uncertainty associated with each method is evaluated. First, the impedance of an air-cored eddy-current coil is measured in the frequency range 100 Hz to 20 kHz. Corrections are made to account for the fact that the coil is not a pure inductor but exhibits finite resistance and capacitance in and between the windings. Then, the conductivity of brass and stainless steel plates is determined with 3 and 2% uncertainty (68% confidence level) by seeking the best fit (least-mean-square error) between experimental measurements of coil impedance and values calculated theoretically. The residual error in the fitting process is found to be the main indicator of uncertainty in the conductivity measurement. Second, four-point alternating current potential drop measurements are made on the same samples in the frequency range 1–100 Hz. Conductivity is determined from these measurements by means of a simple analytic formula, valid in a quasi-static regime, with an uncertainty approximately 0.5%. The main source of uncertainty in the four-point conductivity measurement is scatter in the voltage measurements. Both of these techniques give rise to smaller uncertainties in the measurement of conductivity than a MIZ-21A eddy-current instrument (2% and 40% for brass and stainless steel, respectively) and without the need for calibration specimens. In addition, the four-point approach is independent of magnetic permeability below a certain characteristic frequency and can be used to measure conductivity of ferrous metals. As an example, the conductivity of a spring steel plate is also determined.

Keywords: electrical conductivity measurement, eddy current, four-point, potential drop

1. Introduction

Measurements of electrical conductivity (or resistivity) are useful in metal sorting, alloy identification [1, section 7], heat-treatment monitoring of aluminium alloys [2] and detection of flaws which are manifest as a change in the material conductivity, such as thermal damage in aircraft structures [3]. There is a need for accurate, portable conductivity measurement systems which do not rely on calibration standards.

In this paper, the electrical conductivity of metal plates is measured by two complementary methods. The first relies on broadband measurement, from 100 Hz to 20 kHz, of the impedance change of an air-cored eddy-current coil when the coil is moved from free space to the surface of the metal plate. The method adopted is that described by Harrison *et al*

[4], in which several corrections are made to account for the fact that the coil is not a pure inductor but exhibits finite resistance and capacitance. The conductivity of the metal plate is then determined by seeking the best fit (least-mean-square error) between experimental measurements of coil impedance and values calculated theoretically [5]. This method is well suited for use with non-magnetic metals since the conductivity and permeability cannot be separated unless at frequencies much lower than 40 Hz, which is the lower limit of a typical impedance analyser.

In the second method, measurements of alternating-current potential-drop (ACPD) are made in the frequency range of 1–100 Hz, using a four-point probe. Plate conductivity is then determined by means of a simple analytic formula valid in a quasi-static regime [6]. This method works well for metals but has intrinsically better signal-to-noise ratio for low conductivity materials because the measured voltage is inversely proportional to the material conductivity. In addition, the four-point approach is independent of magnetic permeability below a certain characteristic frequency (dependent on the geometry, conductivity and permeability of the specimen) and can be used for conductivity measurement of ferrous metals. ACPD measurements have the advantage over direct-current potential-drop (DCPD) measurements [7] that the use of alternating current makes it possible for lower measuring current to be applied in order to achieve a given sensitivity [1, section 8]. This reduces the risk of temperature rise in the part under test and associated changes in the material conductivity [8].

The uncertainty associated with each of these techniques is evaluated according to NIST guidelines [9]. For the eddy-current method, the residual error in seeking a fit between measured and calculated impedance data is found to be the main indicator of uncertainty in the measured conductivity. For brass and stainless steel plates, the uncertainty in the conductivity is determined to be 3 and 2% respectively, with a 68% confidence level. The main source of uncertainty in the four-point conductivity measurement is scatter in the voltage measurements. In this case, the conductivity of brass, stainless steel and spring steel plates is determined with uncertainty 0.5, 0.5 and 0.7% respectively. Both of these techniques give rise to smaller uncertainties in the measurement of conductivity than a Zetec MIZ-21A eddy-current instrument (2% and 40% for brass and stainless steel, respectively) and without the need for calibration specimens.

Commercially-available eddy-current conductivity meters are calibrated using sets of reference standards whose conductivity values span a range which includes those of the samples to be measured [2, 3, 8, 10, 11]. All eddy-current methods for conductivity measurement are restricted to use with non-ferrous metals. Sources of error and ways of reducing uncertainty in conductivity measurements using commercially-available eddy-current meters are discussed in [3, 8]. Factors which contribute to the uncertainty in these measurements are variations in specimen geometry and dimensions, probe stand-off from the test-piece, probe temperature, specimen temperature and possible slight magnetic permeability of the specimen. These factors are also important in the eddy-current method described here and are discussed in sections 3 and 5.

Table 1. Plate parameters: conductivity, σ (measured using a Zetec MIZ-21A eddy-current instrument); thickness, T; and lateral dimensions, $w \times l$.

Plate	Alloy	σ (MS m^{-1})	T (mm)	$w \times l$ (mm)
Brass	C26000	16.2 ± 0.3	5.66 ± 0.01	615×616
Stainless steel	316	0.7 ± 0.3	6.36 ± 0.01	457×457
Spring steel	C1074/75	–	1.57 ± 0.01	412×412

In [10], a remarkably accurate and precise eddy-current method for conductivity measurement is described. A linear relationship between conductivity, σ, and angular frequency, ω, is established by keeping the product $\omega\sigma$ constant in all measurements. Then, only one conductivity standard is needed to calibrate the instrument over the range of 1–100% IACS. IACS is an abbreviation for International Annealed Copper Standard, a measure of conductivity used to compare electrical conductors to a traditional copper-wire standard. Conductivity is expressed as a percentage of the standard, so that 100% IACS represents a conductivity of 58 MS m^{-1}. An eddy-current bridge circuit was constructed, with the capability of measuring both real and imaginary parts of impedance accurately. Changes of 0.001% IACS using a 100% IACS standard were detected. The system was, however, difficult to operate and, in the reported form, non-transportable. In [2, 11], the resistivity of rectangular annuli was measured with an uncertainty between 0.4 and 0.7% utilizing a Heydweiller bridge arrangement. The purpose was to produce sets of reference blocks for calibration of eddy-current conductivity meters [11]. In contrast with these bridge approaches, the ACPD method described in this paper offers the potential of achieving less than 1% uncertainty in measurements of σ in an easily-portable and easy-to-use system.

2. Metal plates

Three plates were studied: brass, stainless steel and spring steel. These give a range of conductivity from approximately 1 to 20 MS m^{-1}, with spring steel also being strongly ferromagnetic. Parameters of the plates are given in table 1. The brass plate was precision ground on receipt to remove surface scratches. The stainless steel plate was received in precision-ground form. The spring steel plate was received in cold-rolled form, completely annealed. It was demagnetized on receipt in both horizontal axes, using a demagnetizing coil. The plate conductivity values listed in table 1 were obtained using a Zetec MIZ-21A eddy-current instrument. The manufacturer's statement of uncertainty of the instrument was used to obtain the uncertainty values quoted in table 1. For materials with conductivity in the ranges of 0.9–25% and 16–60% IACS, the uncertainty in the conductivity measurement is ±0.5% IACS. It is not possible to measure the conductivity of ferrous metals, such as spring steel, with this instrument. Plate thicknesses were measured using digital calipers at several points around the plate edges. The mean values are listed in table 1. The horizontal dimensions of the plates were sufficiently large that edge effects were not

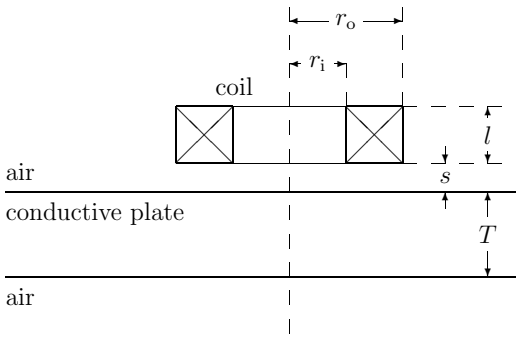

Figure 1. Cross-section through the axis of a circular, air-cored, eddy-current coil, positioned horizontally above a metal plate.

measurable by either the eddy-current or four-point ACPD probe, when centred on the plates.

3. Eddy-current conductivity measurement method

Plate conductivity was measured by placing a well-characterized, air-cored eddy-current probe in contact with the plate, with the axis perpendicular to the plate, and measuring the impedance of the coil over the frequency range 100 Hz to 20 kHz. The measured data were compared with the well-established theory of Dodd and Deeds [5] in order to determine the plate conductivity. Following the method presented by Harrison *et al* [4], several corrections were applied in order to account for non-ideal coil behaviour. These are described in section 3.3. The probe and specimen were both allowed to reach ambient temperature prior to carrying out measurements. It is assumed that the sample temperature did not significantly change during the course of each measurement.

3.1. Coil impedance change due to a planar conductor

For a circular eddy-current coil with rectangular cross-section, as shown in figure 1, closed-form solutions are given in [5]. Expressions relevant to this work are reproduced here. It is assumed that the current density across the rectangular cross-section of the coil is uniform, driven by alternating current of constant amplitude, such that $I(t) = \mathrm{Re}(I\,\mathrm{e}^{-\mathrm{i}\omega t})$, with $\omega = 2\pi f$ being the angular frequency. In the closed-form solutions of [5], it is also assumed that the resistance of the coil is negligible. Hence, no resistive terms appear in equations (1) and (3). This omission is dealt with by applying a correction to the experimental data, described in section 3.3.1.

The coil impedance in air, Z_{air}, is given by

$$Z_{\mathrm{air}} = \frac{2\mathrm{i}\pi\omega\mu_0\mathsf{n}^2}{l^2(r_o - r_i)^2}\int_0^\infty \frac{I^2(\kappa r_o, \kappa r_i)}{\kappa^5}\left(l + \frac{\mathrm{e}^{-\kappa l} - 1}{\kappa}\right)\mathrm{d}\kappa. \quad (1)$$

In equation (1), μ_0 is the permeability of free space (assumed equal to that of air), n is the number of turns on the coil, r_o is the outer radius, r_i the inner radius and l the length of the coil. Further,

$$I(b, a) = \int_a^b x J_1(x)\,\mathrm{d}x,$$

where $J_1(x)$ is the first-order Bessel function of the first kind. The coil inductance, L_0, may be obtained simply from the relation

$$\omega L_0 = |Z_{\mathrm{air}}|. \quad (2)$$

The impedance of a coil whose base is a distance s above the surface of a magnetic conductive plate, relative permeability μ_r, conductivity σ and thickness T, is given by

$$Z = \frac{\mathrm{i}\pi\omega\mu_0\mathsf{n}^2}{l^2(r_o - r_i)^2}\int_0^\infty \frac{I^2(\kappa r_o, \kappa r_i)}{\kappa^5} \times \left(2l + \frac{1}{\kappa}\left\{2\mathrm{e}^{-\kappa l} - 2 + [\mathrm{e}^{-2\kappa(l+s)} + \mathrm{e}^{-2\kappa s} - 2\mathrm{e}^{-\kappa(l+2s)}] \times \left[\frac{(\gamma^2 - \mu_r^2\kappa^2)(1 - \mathrm{e}^{2\gamma T})}{(\gamma^2 + \mu_r^2\kappa^2)(1 - \mathrm{e}^{2\gamma T}) - 2\mu_r\kappa\gamma(1 + \mathrm{e}^{2\gamma T})}\right]\right\}\right)\mathrm{d}\kappa, \quad (3)$$

in which $\gamma^2 = \kappa^2 - \mathrm{i}\omega\mu_0\mu_r\sigma$. Equation (3) results from a straightforward adaptation of the theory of [5], for a non-magnetic half-space conductor with a surface layer.

3.2. Coil fabrication

The probe former and sleeve were machined from delrin. A spur at the top of the former was machined to fit inside the chuck on a coil winder. The coil was wound in layers, the windings as regular as possible, and the number of turns at each layer was recorded. Once the coil was wound, its free-space impedance was measured at 40, 100 and 1000 Hz by connecting the ends of the wire directly to an Agilent 4294A impedance analyser. The wire ends were then soldered to a 10–32 (microdot) feed-through connector, which was mounted in the spur at the top of the former. This connector permits the probe to be connected to the current source by means of a coaxial cable with 10–32 plug at one end and BNC plug at the other. The impedance of the probe was then re-measured to check that the connections were good. Once it had been determined that no appreciable change in the coil impedance had occurred due to the soldered joint, the former (to cover the windings) was put in place and fixed by setting with a plastic potting compound. The compound was allowed to dry thoroughly over a period of several days. The base of the probe was then machined down to give a nominal stand-off (distance between the base of the coil and base of the probe), s, of 1 mm. The machining was done parallel with the base of the former, which was found to list by approximately 0.04 mm with respect to the sleeve. After machining, it was observed that the face of the former became cupped (by approximately 0.04 mm from the centre to the edge) due to pressure from the coil windings. The measured parameters of the coil are given in table 2. The inner radius and length of the coil were obtained by measuring the dimensions of the delrin former using digital calipers, before the coil was wound. The outer radius of the coil was measured using digital calipers, before the sleeve was placed over the wound coil. The self-inductance, dc resistance and resonant frequency of the coil were measured using an Agilent 4294A impedance analyser, taking the low-frequency limit to obtain L_0 and R_0.

Table 2. Measured coil parameters. Lengths were measured using digital calipers at appropriate stages during fabrication of the coil. L_0, R_0 and f_r were measured using an Agilent 4294A impedance analyser, taking the low-frequency limit to determine L_0 and R_0.

r_i	Inner radius (mm)	4.04 ± 0.01
r_o	Outer radius (mm)	11.84 ± 0.01
l	Length (mm)	8.02 ± 0.01
s	Stand-off (mm)	1.00 ± 0.02
n	Number of turns	1858
L_0	Self-inductance (mH)	33.9
R_0	DC resistance (Ω)	80.1
f_r	Resonant frequency (kHz)	191

3.3. Corrections for non-ideal coil behaviour

In practice, the current flowing in an eddy-current coil is not uniformly distributed over the cross section of the coil. The current is restricted to flow in the windings, in fact near the surface of the windings for higher frequencies—a consequence of the skin effect. Restriction of the current in this way causes the coil to exhibit inter-wire capacitance. The fact that the wire is not perfectly conducting means that the coil also exhibits dc resistance. Additional perturbations to the current density in the coil arise from irregularity in the windings. Capacitance associated with the leads can also be problematic. Theoretically, the coil is modelled as a pure inductor and, in order to achieve good agreement between experimental measurements and theoretical calculations of coil impedance, it is necessary to correct for the non-ideal behaviour of the coil.

3.3.1. DC coil resistance and stray capacitance. Following the method described in [4], the experimental data were corrected to eliminate the effects of stray capacitance and dc resistance of the coil. The ideal admittance, obtained from the dc values of coil resistance and inductance, R_0 and L_0 respectively, is

$$Y_0 = \frac{1}{Z_0} = \frac{1}{R_0 - i\omega L_0}. \tag{4}$$

Subtracting Y_0 from the admittance in air,

$$Y_{air}^{exp} = \frac{1}{Z_{air}^{exp}}, \tag{5}$$

gives the admittance of the equivalent parallel network, Y_P, which must be corrected for;

$$Y_P = Y_{air}^{exp} - Y_0. \tag{6}$$

Denoting the uncorrected impedance of the coil, measured with the coil over the conductive plate, by Z_U^{exp} (with the associated admittance Y_U^{exp}), the corrected impedance Z_C^{exp} is given by

$$Z_C^{exp} = \frac{1}{Y_U^{exp} - Y_P}. \tag{7}$$

The corrected impedance change in the coil due to the plate, ΔZ_C^{exp}, is therefore

$$\Delta Z_C^{exp} = Z_C^{exp} - Z_0. \tag{8}$$

In the case that this correction procedure is not followed, the impedance change in the coil due to the plate is given by

$$\Delta Z_U^{exp} = Z_U^{exp} - Z_0. \tag{9}$$

3.3.2. Effective coil parameters and determination of plate conductivity. Calculating the self-inductance of the coil using equations (1) and (2), with the measured coil dimensions r_i, r_o and l given in table 2, yields $L_0 = 34.8$ mH. This value is 3% higher than the measured value listed in table 2. The discrepancy can be explained by arguing that the measured value of r_o over-estimates the equivalent value for an ideal coil, since it represents the outermost extent of the windings of a non-uniform current distribution. An equivalent but uniform current distribution would occupy a smaller volume than the real, non-uniform current distribution in the coil. Perfect agreement between the calculated and measured values of L_0 can be obtained by introducing an effective value for the coil outer radius, $r_o^{eff} < r_o$. The value of r_o^{eff} was determined by varying its value in the calculation of L_0 until agreement with the measured value was achieved. In this way, the result $r_o^{eff} = 11.43 \pm 0.06$ mm was obtained. The uncertainty in this value derives from the accuracy of the impedance analyser at the lower end of its operating frequency range, which is 0.5% (table 5).

Again due to non-uniformity of the current density in the coil, it is anticipated that the measured stand-off of the coil will be smaller than that of an ideal coil for which other parameters are identical. An effective value of the coil stand-off may be determined by minimizing the root-mean-square (RMS) error between the experimentally measured impedance of the coil on a metal plate, and values calculated using equation (3). The RMS error, ε, is computed from the following relation, in which the superscript 'exp' denotes experimentally measured values, and 'thry' denotes theoretically calculated values. N is the number of frequency points.

$$\varepsilon^2 = \frac{1}{N}\sum_{j=1}^{N}\left\{\left[\frac{\Delta R_j^{exp}(f_j) - \Delta R_j^{thry}(f_j)}{\Delta R_j^{exp}(f_j)}\right]^2 + \left[\frac{\Delta L_j^{exp}(f_j) - \Delta L_j^{thry}(f_j)}{\Delta L_j^{exp}(f_j)}\right]^2\right\}. \tag{10}$$

At the same time, the conductivity of the plate is permitted to vary until ε is minimized. The probe stand-off and plate conductivity may be found simultaneously since ε shows well-defined minima with respect to variations in both of these parameters [4].

In figure 2, the corrected experimental data, ΔZ_C^{exp} of equation (8), and uncorrected experimental data, ΔZ_U^{exp} of equation (9), are shown for normalized coil impedance change due to the brass plate. Also shown are the curves calculated using equation (3) with measured and effective parameters, table 3. The improvement in agreement between theory and experiment after making corrections for dc coil resistance and stray capacitance, section 3.3.1, and refining coil parameters r_o and s, as described in this section, is dramatic. Similar curves are obtained for the stainless steel plate, not shown here.

In table 3, effective parameters obtained by this procedure are compared with dimensions measured using digital calipers and conductivities measured using the Zetec MIZ-21A eddy-current instrument. The value of ε obtained for the experiment on brass was 0.03, or 3%. For stainless steel, $\varepsilon = 2\%$. In both cases $N = 100$, covering the frequency range 1.8–20 kHz logarithmically. The uncertainties in the effective values of s

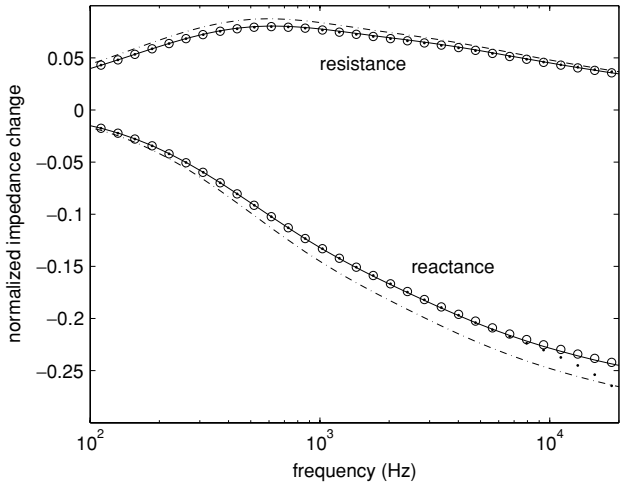

Figure 2. Change in coil impedance due to the brass plate, normalized to the ideal isolated coil reactance $X_0 = \omega L_0$. ○, experimental data corrected for non-ideal coil behaviour; ·, uncorrected experimental data; ——, theory with effective parameters; — · —, theory with measured parameters (tables 2 and 3).

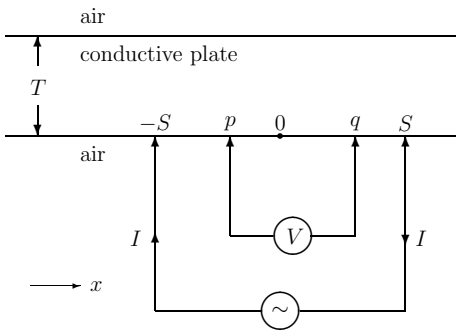

Figure 3. A four-point probe in contact with a conductive plate. The contact points are arranged on a straight line. I is the amplitude of the applied alternating current.

Table 3. Measured and effective parameters. Lengths were measured using digital calipers at appropriate stages during fabrication of the coil. σ was measured using a Zetec MIZ-21A eddy-current instrument.

Parameter		Measured	Effective
r_o	Outer radius (mm)	11.84 ± 0.01	11.43 ± 0.06
s	Stand-off (mm)		
	Brass	1.00 ± 0.04	1.06 ± 0.03
	Stainless steel	1.00 ± 0.04	1.01 ± 0.02
σ	Conductivity (MS m^{-1})		
	Brass	16.2 ± 0.3	16.6 ± 0.4
	Stainless steel	0.7 ± 0.3	1.31 ± 0.02

and σ, quoted in table 3, were assumed equal to ε for each plate.

4. Four-point ACPD conductivity measurement

Consider the schematic diagram of a four-point probe in contact with a conductive plate, figure 3. Elsewhere [6] it has been derived that, for this configuration, the voltage V measured between pick-up points at p and q can be expressed as

$$V = \frac{I}{2\pi\sigma T} \ln\left[\frac{(S-p)(S+q)}{(S+p)(S-q)}\right], \qquad f < f_s. \tag{11}$$

This equation is determined through a series expansion analysis of an expression valid at arbitrary frequency. It represents a quasi-static regime in which the measured voltage is approximately real and constant, bounded by frequency f_s whose value is chosen depending on the level of accuracy required. For 0.1% accuracy,

$$f_s = \frac{3}{20\sqrt{2}\pi\mu\sigma T^2}. \tag{12}$$

In equations (11) and (12), I is the amplitude of the alternating current, σ and μ are the conductivity and magnetic permeability of the plate, respectively, and T is the plate thickness.

For equally-spaced contact points, equation (11) reduces to

$$V = \frac{I}{\pi\sigma T} \ln 2, \tag{13}$$

in agreement with the static result of [7, part 5, equation (6)], valid for a plate thickness somewhat smaller than the separation of the probe points.

Table 4. Probe parameters.

S (mm)	25.454 ± 0.005
p (mm)	-10.152 ± 0.005
q (mm)	10.162 ± 0.005

4.1. Probe

Four sprung, point contacts were mounted in a plastic support block. The four points were arranged along a straight line, and the separation of the contacts was measured using a travelling microscope. With reference to figure 3, the dimensions of the probe are listed in table 4.

4.2. Voltage measurement

The metal plates were mounted on a 5 cm thick plastic support plate. The four-point probe was fixed in contact with the metal surface, to the specified travel distance of the sprung contacts. The two pick-up wires were arranged with the objective of minimizing the inductance in the measurement circuit, which becomes significant at frequencies greater than f_s. The wires run along the underside of the plastic block housing the pick-up contacts, lying as close to the plate surface as possible. They were twisted together at the midpoint between the pick-up points.

For the determination of plate conductivity, two measured values are required. One is the current through the plate, I, and the other is the voltage between the pick-up points, V. To monitor the current in the plate, a high-precision resistor was connected in series with the drive-current circuit, and the voltage across the resistor was measured. The resistor was characterized in advance by measuring its resistance R over the frequency range 40 Hz to 40 kHz using an Agilent 4294A precision impedance analyser. The uncertainty in the value of R, given in table 5, derives from the accuracy of the impedance

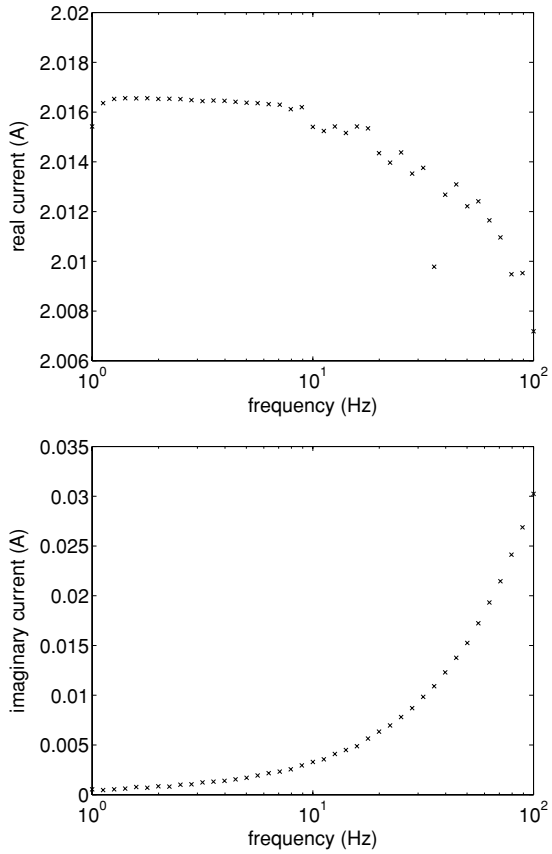

Figure 4. Measured current in the plate.

Table 5. Accuracy of the Agilent 4294A at various frequencies, and R.

Frequency	Accuracy (%)
40 Hz	0.5
400 Hz	0.3
4 kHz	0.1
40 kHz	0.1
60 kHz	0.3
R (mΩ)	98.7 ± 0.5

analyser, also given in table 5 for various frequencies, since the uncertainty due to scatter in the measured values of R was only 0.03%.

The voltages across the resistor and between the pick-up points were both measured using a Stanford Research Systems SR830 DSP lock-in amplifier. In order to make both voltage measurements using the same lock-in amplifier, a switch was activated by a control signal from the auxiliary analogue output of the lock-in amplifier. The current in the plate was maintained as close to 2 A as possible over the frequency range of the experiment. In practice, the real and imaginary parts of the current varied as shown in figure 4.

It was necessary to correct the experimental data for common-mode rejection (CMR) error in the lock-in amplifier. This systematic error shows itself in the fact that, when the pick-up terminals are reversed, the measured voltage changes by a few μV. The magnitude of the error is, for the non-magnetic plates, similar to that of the voltage being measured

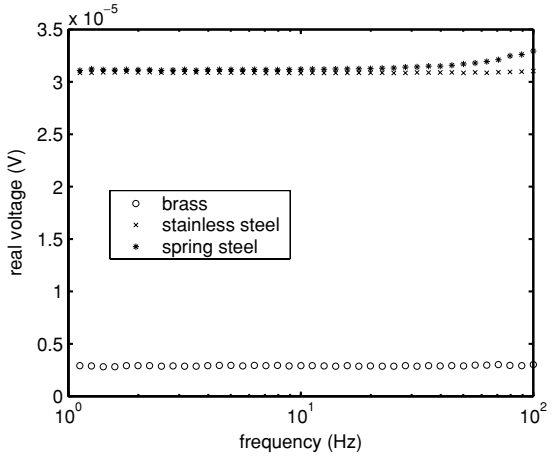

Figure 5. Measured ACPD voltage.

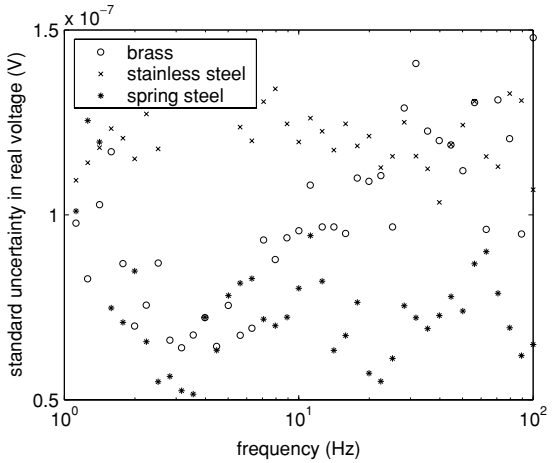

Figure 6. Standard uncertainty in the measured ACPD voltage.

and a corrective procedure is essential. The CMR error was eliminated by taking two sets of measurements, reversing the pick-up terminals in between, and averaging. The standard error in the measurement data was reduced by taking ten sets of measurements at each frequency and then determining the mean value. Measured voltages for the three plates are shown in figure 5. The standard uncertainty in measurements for each of the plates is shown in figure 6.

The drive current was produced by a Kepco bipolar operational power supply/amplifier, model number BOP 20-20M. The sine signal from the internal function generator of the lock-in amplifier was connected to the current programming input of the power supply, with the power supply working as a current driver.

4.3. Plate conductivity and uncertainty analysis

An expression for the conductivity of the plate can be obtained by simple rearrangement of equation (11):

$$\sigma = \frac{V_R}{2\pi RVT} \ln\left[\frac{(S-p)(S+q)}{(S+p)(S-q)}\right], \qquad f < f_s, \quad (14)$$

where the substitution $I = V_R/R$ has been made so that equation (14) contains the quantities that are measured experimentally.

Table 6. Mean measured voltage values and number of data points, n. V_R is measured across a high-precision resistor for the purpose of monitoring the current applied to the plate. V is the pick-up voltage measured across points $x = p, q$ on the plate, figure 3.

Plate	V_R (mV)	V (μV)	n
Brass	198.6 ± 0.1	5.83 ± 0.01	34
Stainless steel	198.80 ± 0.05	62.24 ± 0.01	40
Spring steel	199.000 ± 0.008	62.84 ± 0.01	23

Table 7. Plate conductivity (MS m^{-1}), measured using a commercial instrument, the eddy-current method of section 3 and the four-point ACPD method of section 4.

Plate	Zetec MIZ-21A	Eddy current	ACPD
Brass	16.2 ± 0.3	16.6 ± 0.4	16.42 ± 0.09
Stainless steel	0.7 ± 0.3	1.31 ± 0.02	1.369 ± 0.007
Spring steel	–	–	5.50 ± 0.04

For each of the plates, values of V_R and V were obtained by taking the mean of the values measured in the frequency ranges 1–50 Hz for brass, 1–100 Hz for stainless steel and 1–15 Hz for spring steel, according to calculated values of f_s, equation (12), for each plate. Note that the relative permeability of the spring steel plate has previously been measured as $\mu_r = 134 \pm 3$ [6]. It is noticeable from figure 5 that the voltage measured on the spring steel plate departs from a constant value at a few tens of Hertz, in accordance with the value $f_s \approx 15$ Hz for this plate. The mean voltage values obtained, and uncertainties in those values, are listed in table 6. The uncertainty in the measured voltage was calculated by means of equation (A.5), given in the appendix. Putting these mean measured voltage values into equation (14), with other parameter values given previously, yields the ACPD conductivity values listed in table 7. The uncertainty in the conductivity was computed by applying relation (A.3) to equation (14). The most significant contribution to the uncertainty in these conductivity values was from scatter in the voltage measurements. The uncertainty in the value of the plate thickness was less important for the three plates studied here, but may become dominant for thinner plates. The uncertainty in the dimensions of the four-point probe did not contribute significantly to the over-all uncertainty in σ.

5. Summary and discussion

Conductivity values measured using the Zetec MIZ-21A eddy-current instrument, the eddy-current method described here in section 3 and the ACPD method described in section 4 are compared in table 7. The conductivity values obtained by each of the three measurement methods agree, within experimental uncertainty, in the case of the brass plate, whereas those obtained for stainless steel do not. The disagreement observed in the case of stainless steel is likely due to the fact that this type of stainless steel is often weakly ferromagnetic. For this plate, μ_r has been measured previously using the ACPD technique in the frequency range 100 Hz to 10 kHz [6], giving $\mu_r = 1.06 \pm 0.02$. To test this hypothesis, values of conductivity and stand-off were computed from the eddy-current impedance data for various values of relative

Table 8. Conductivity of stainless steel and associated refinements to the coil stand-off, s^{eff}, obtained using the eddy-current method of section 3, assuming various values of μ_r.

μ_r	σ (MS m^{-1})	s^{eff} (mm)	ε (%)
1.00	1.31 ± 0.02	1.01 ± 0.02	2
1.02	1.379 ± 0.007	1.053 ± 0.005	0.5
1.04	1.45 ± 0.02	1.10 ± 0.01	1
1.06	1.51 ± 0.04	1.14 ± 0.03	3

Table 9. Relative uncertainty in plate conductivity (%).

Plate	Zetec MIZ-21A	Eddy current	ACPD
Brass	2	3	0.5
Stainless steel	40	2	0.5
Spring steel	–	–	0.7

permeability, μ_r, of the stainless steel. The results are shown in table 8. It is clear that the RMS error is minimum (0.5%), out of the four cases considered here, for the value $\mu_r = 1.02$. In this case, the value of conductivity obtained, $\sigma = 1.379 \pm 0.007$ MS m^{-1}, agrees with that obtained by the ACPD measurement method, to within experimental uncertainty. The effective value of the stand-off, $s^{\text{eff}} = 1.053 \pm 0.005$ mm, also agrees with the value obtained for the eddy-current measurements on the brass plate, within experimental uncertainty. These findings support the hypothesis that the stainless steel plate is slightly ferromagnetic, and highlights the sensitivity of the eddy-current conductivity measurement method to changes in μ_r. This point is discussed in [8], in which it is suggested that material relative permeability slightly greater than unity can lead to significant under-estimation of the material conductivity in measurements with commercial eddy-current instruments, for frequencies lower than a few hundred kilohertz.

The relative uncertainty in the conductivity measurement for each method is listed in table 9. It can be seen that, for good non-magnetic conductors such as brass, the performance of the commercial instrument and the eddy-current method detailed here is similar, with uncertainty 2 or 3%. For low-conductivity metals such as stainless steel, however, the commercial instrument performs poorly by comparison. In all cases, the four-point ACPD method yields the smallest uncertainties, 0.5 and 0.7%. These uncertainties compare well with those reported in [2, 11] (between 0.4 and 0.7%), in which a Heydweiller-bridge eddy-current measurement system is used. In contrast with the Heydweiller bridge arrangement, however, the four-point ACPD measurement system is easy to use and interpretation of the measurements is straightforward.

Further improvement in reducing the uncertainty associated with the ACPD technique may be made by using a resistor whose resistance is prescribed with high accuracy, to improve upon the 0.5% uncertainty associated with measuring the value of R using an impedance analyser, as performed here. Reduction of the uncertainty in the value of the plate thickness, by an order of magnitude, can be achieved by using a digital indicator rather than digital calipers for this measurement.

The four-point ACPD method may be developed for use with other sample geometries, for example cylindrical

surfaces, by derivation of the appropriate expression for the measured voltage—equivalent to equation (11) used here for the plate geometry. This is planned for future work.

Acknowledgments

This work was supported by the NSF Industry/University Cooperative Research program. The authors thank J R Bowler and M J Johnson for helpful comments regarding the experiments. NB thanks T P Theodoulidis for suggesting useful references and S K Burke for commenting on the manuscript.

Appendix

In this appendix, relationships used for determining measurement uncertainties according to the guidelines of [9] are summarized.

Consider a measurand Y, determined from N other quantities $X_1, X_2, \ldots, X_N$ through a functional relation f:

$$Y = f(X_1, X_2, \ldots, X_N). \tag{A.1}$$

An estimate of the measurand Y, denoted by y, is obtained from (A.1) using input estimates $x_1, x_2, \ldots, x_N$ for the values of the N input quantities. Thus the result of the measurement is given by

$$y = f(x_1, x_2, \ldots, x_N). \tag{A.2}$$

The combined standard uncertainty of the measurement result y, denoted by $u_c(y)$, may be determined from

$$u_c^2(y) = \sum_{i=1}^{N} \left(\frac{\partial f}{\partial x_i} \right)^2 u^2(x_i), \tag{A.3}$$

commonly referred to as the law of propagation of uncertainty. Sensitivity coefficients $\partial f/\partial x_i$ are equal to $\partial f/\partial X_i$ evaluated at $X_i = x_i$. $u(x_i)$ is the standard uncertainty associated with the input estimate x_i. In the form given in equation (A.3), the contribution to $u_c(y)$ due to estimated covariances associated with quantities x_i and x_j is assumed negligible.

For an input quantity X_i whose value is estimated from n independent observations $X_{i,k}$, x_i is the sample mean,

$$x_i = \overline{X}_i = \frac{1}{n} \sum_{k=1}^{n} X_{i,k}, \tag{A.4}$$

and the standard uncertainty $u(x_i)$ associated with x_i is the estimated standard deviation of the mean:

$$u^2(x_i) = s^2(\overline{X}_i) = \frac{1}{n(n-1)} \sum_{k=1}^{n} (X_{i,k} - \overline{X}_i)^2. \tag{A.5}$$

References

[1] Moore P O, McIntire P (eds) and Stanley R K (technical ed) 1995 Special nondestructive testing methods *Nondestructive Testing Handbook* 2nd edn, vol 9 (Columbus, OH: American Society of Nondestructive Testing)

[2] Lynch A C, Drake A E and Dix C H 1983 Measurement of eddy-current conductivity *IEE Proc.* A **130** 254–60

[3] Metcalfe G R 1988 The use of eddy current flaw detectors with meter display for measuring the conductivity of aluminium alloy structures *Br. J. NDT* **30** 164–9

[4] Harrison D J, Jones L D and Burke S K 1996 Benchmark problems for defect size and shape determination in eddy-current nondestructive evaluation *J. Nondestr. Eval.* **15** 21–34

[5] Dodd C V and Deeds W E 1968 Analytical solutions to eddy-current probe-coil problems *J. Appl. Phys.* **39** 2829–38

[6] Bowler N and Huang Y 2005 Model-based characterization of homogeneous metal plates using four-point alternating current potential drop measurements *IEEE Trans. Magn.* **41** 2102–10

[7] Moore P O (ed) and Udpa S S (technical ed) 2004 Electromagnetic testing *Nondestructive Testing Handbook* 3rd edn, vol 5 (Columbus, OH: American Society of Nondestructive Testing)

[8] Suhr H and Guettinger T W 1993 Error reduction in eddy current conductivity measurements *Br. J. NDT* **35** 634–8

[9] Taylor B N and Kuyatt C E 1994 Guidelines for evaluating and expressing the uncertainty of NIST measurement results *NIST Technical Note* 1297

[10] Free G 1981 High-accuracy conductivity measurements in nonferrous metals *Eddy-Current Characterization of Materials and Structures* ed G Birnbaum and G Free (Philadelphia, PA: ASTM) STP 722, pp 121–8

[11] Drake A E and Lynch A C 1987 AC conductivity standards for the calibration of eddy-current conductivity meters *J. Phys. E: Sci. Instrum.* **20** 137–9